Finite Element Method for High-Speed Flow-Structure Interaction

W. Limtrakarn[1] and P. Dechaumphai[2]

[1]Department of Mechanical Engineering, Faculty of Engineering, Thammasat University, Bangkok 12121, Thailand.
Tel: +66-(0)-2564-3001-9, Fax: +66-(0)-2564-3010, E-mail: limwiroj@engr.tu.ac.th[1]
[2]Department of Mechanical Engineering, Faculty of Engineering, Chulalongkorn University, Bangkok 10330, Thailand.

Abstract

The finite element method for two-dimensional high-speed flow-structure interaction is presented. The adaptive cell-centered finite element method was used to solve the Navier-Stokes equations for high-speed flow analysis. The Galerkin method was then used to develop the finite element equations for analyses of the transient heat transfer and the structural response from the energy equation and the equilibrium equations, respectively. Finally, the coupled high-speed flow-structure problem was used to demonstrate the effectiveness of the proposed finite element method for predicting interdisciplinary fluid-thermal-structural interaction phenomena.

1. Introduction

Design of high-speed flight vehicles requires accurate prediction of flow phenomena, aerodynamic heating rates on the structural surfaces, structural temperature and their gradients, as well as structural deformations and stresses. High-speed flow phenomena normally include complex flow characteristics, such as shock waves, shock-shock interactions, thin boundary layers and shock-boundary layer interactions [1,2]. Some of these characteristics especially near the structural surface, generate aerothermal load through vehicle structure and normally affect the structural temperature, deformation and stress. In a few second, structural temperatures begin to rise and significant deformations occur. In addition, the deformed structure can alter high-speed flow behavior and thus the aerothermal loads. These coupled effects indicate that the analysis of high-speed flow-structure interaction [3] is an important consideration for high-speed vehicle design.

In this paper, an integrated flow, thermal, and structural analysis approach for predicting each disciplinary behavior and their interactions is presented. For high-speed compressible flow, the cell-centered finite element method is combined with the adaptive meshing technique [4,6] to solve the Navier-Stokes equations. Based on the solution obtained from the previous mesh, the adaptive meshing technique generates an entirely new mesh that consists of small elements in the regions with large change in solution gradients and large elements in the other regions where the change in solution gradients are small. The combined technique is used to improve the efficiency of the finite-element flow solution and the aerothermal loads, as well as to reduce the computational time and the computer memory. The Galerkin finite element method is applied to solve the structural energy equation for temperature distribution and the structural equations for deformations and stresses. The paper starts by explaining the theoretical formulation of high-speed compressible flow, structural heat transfer, and structural response. Then the solution procedure for flow-thermal-structural interaction problem is presented. Finally, the integrated approach is evaluated by analyzing the application of Mach 10 flow over an inclined plate.

2. Theoretical Formulation

2.1 Governing Differential Equations

The equations for the high-speed compressible flow, the structural heat transfer, and the structural analysis in two dimensions are described below.

2.1.1 High-speed compressible flow

The equations for high-speed viscous compressible flow are represented by the conservation of mass, momentums, and energy. These equations are written in the conservation form [7] as,

$$\frac{\partial}{\partial t}\{U_F\} + \frac{\partial}{\partial x}\{E_F\} + \frac{\partial}{\partial y}\{F_F\} = 0 \qquad (1)$$

where the subscript F denotes the fluid analysis. The vector $\{U_F\}$ contains the fluid conservation variables defined by,

$$\{U_F\} = \begin{Bmatrix} \rho \\ \rho u \\ \rho v \\ \rho \varepsilon \end{Bmatrix} \quad (2)$$

where ρ is the fluid density, u and v are the velocity components in the x and y directions, respectively, and ε is the total energy. The vectors $\{E_F\}$ and $\{F_F\}$ consist of the flux components in the x and y directions, respectively. These flux vectors are given by,

$$\{E_F\} = \{E_I\} - \{E_V\}$$

$$= \begin{Bmatrix} \rho u \\ \rho u^2 + p \\ \rho uv \\ \rho u\varepsilon + pu \end{Bmatrix} - \begin{Bmatrix} 0 \\ \sigma_x \\ \tau_{xy} \\ u\sigma_x + v\tau_{xy} - q_x \end{Bmatrix} \quad (3)$$

$$\{F_F\} = \{F_I\} - \{F_V\}$$

$$= \begin{Bmatrix} \rho v \\ \rho uv \\ \rho v^2 + p \\ \rho v\varepsilon + pv \end{Bmatrix} - \begin{Bmatrix} 0 \\ \tau_{xy} \\ \sigma_y \\ u\tau_{xy} + v\sigma_y - q_y \end{Bmatrix} \quad (4)$$

The subscripts I and V represent the inviscid and viscous flux vector components, respectively. In the inviscid flux components, the pressure p is related to the total energy assuming a calorically perfect gas. In the viscous flux components, the stresses σ_x, σ_y, and τ_{xy} are related to the velocity gradients assuming the Stokes' hypothesis [8].

2.1.2 Structural heat transfer

The thermal response of the structure is described by the energy equation in the conservation form as,

$$\frac{\partial}{\partial t}(U_T) + \frac{\partial}{\partial x}(E_T) + \frac{\partial}{\partial y}(F_T) = (G_T) \quad (5)$$

where the subscript T denotes the structural heat transfer analysis. The vector U_T contains the thermal conservation variable defined by,

$$U_T = \rho cT \quad (6)$$

where c is the specific heat of structure, G_T is the heat source and the heat flux components E_T and F_T are,

$$E_T = -k\frac{\partial T}{\partial x} \quad (7)$$

$$F_T = -k\frac{\partial T}{\partial y} \quad (8)$$

2.1.3 Structural response

The structural response is governed by the quasi-static equilibrium equations given by,

$$\frac{\partial}{\partial x}\{E_S\} + \frac{\partial}{\partial y}\{F_S\} = 0 \quad (9)$$

where the subscript S denotes the structural analysis. The flux vector components $\{E_S\}$ and $\{F_S\}$ are,

$$\{E_S\} = \begin{Bmatrix} \sigma_x \\ \tau_{xy} \end{Bmatrix} \quad (10)$$

$$\{F_S\} = \begin{Bmatrix} \tau_{xy} \\ \sigma_y \end{Bmatrix} \quad (11)$$

where the stress components σ_x, σ_y, and τ_{xy} are related to the strain and the temperature by the generalized Hook's law [5].

2.2 Finite Element Formulation

The cell-centered finite element method is applied to the Navier-Stokes equations to derive the finite element equations. The Galerkin finite element approach is applied to the structural heat transfer equation and the equilibrium equations to derive the corresponding finite element equations. The derivation procedures are briefly described below,

2.2.1 Finite-element flow equations

The method of weighted residuals [9] is applied to Eq. (1), over the element domain, Ω, by using unit interpolation function as,

$$\int_\Omega \frac{\partial}{\partial t}\{U_F\}\,d\Omega = -\int_\Omega \frac{\partial}{\partial x}\{E_F\}\,d\Omega - \int_\Omega \frac{\partial}{\partial y}\{F_F\}\,d\Omega \quad (12)$$

The Gauss divergence theorem is then applied to the flux integral terms of Eq. (12) to yield,

$$\int_\Omega \frac{\partial}{\partial x}\{E_F\}\,d\Omega + \int_\Omega \frac{\partial}{\partial y}\{F_F\}\,d\Omega = \int_{\Gamma_e}(\{G_I\} + \{G_V\}) \bullet \hat{n}\,d\Gamma \quad (13)$$

where the flux vectors $\{G_I\}$ and $\{G_V\}$ are the inviscid and viscous flux vectors of $\{E_I + F_I\}$ and $\{E_V + F_V\}$, respectively, and $\hat{n}$ is the unit vector normal to the element boundary Γ_e. Equation (13) is evaluated by summing the normal fluxes from all the sides, Γ_e, of the element. The fluxes normal to the element sides are then approximated by the numerical inviscid and viscous fluxes, $\{\overline{G}_I\}$ and $\{\overline{G}_V\}$, which are the average quantities normal to the element sides, i.e.,

$$\int_{\Gamma_e} (\{G_I\} + \{G_V\}) \bullet \hat{n} d\Gamma = \sum_S \delta_S (\{\overline{G}_I\} + \{\overline{G}_V\}) \qquad (14)$$

where δ_S is the length of element side being considered as shown in Fig. 1, and the summation is performed for all the sides.

By substituting Eq. (14) into Eqs. (13) and (12), then applying an explicit time marching algorithm [7], Eq. (12) becomes,

$$\frac{A_e}{\Delta t}\{U_F^{n+1} - U_F^n\} = -\sum_S \delta_S (\{\overline{G}_I\} + \{\overline{G}_V\}) \qquad (15)$$

where $\{U_F\}^{n+1}$ and $\{U_F\}^n$ are the conservation variables at time steps n+1 and n, respectively, Δt is the time step, and A_e is the element area.

The basic concept behind the cell-centered finite element method used in this paper is to determine the flux across element interfaces by Roe's averaging procedure [6]. The average inviscid flux $\{\overline{G}_I\}$ is given by,

$$\{\overline{G}_I\} = \frac{1}{2}\left[\{G_I^L\} + \{G_I^R\} + |A^*|(\{U_F^L\} - \{U_F^R\})\right] \qquad (16)$$

where the superscripts L and R denote the left and right elements, respectively. The last term in Eq. (16) may be viewed as artificial diffusion needed for solution stability. This diffusion is represented by the product of the Jacobian matrix $|A^*|$ and the difference between the left and right element conservation variables $\{U_F^L\}$ and $\{U_F^R\}$.

By substituting Eq. (16) into Eq. (15), the increments of the conservation variables, $\{\Delta U_F\} = \{U_F\}^{n+1} - \{U_F\}^n$, can be computed explicitly from,

$$\frac{(\{U\}^{n+1} - \{U\}^n)A_e}{\Delta t} = -\frac{1}{2}\sum_S \delta_S\left[\{G_I^L\} + \{G_I^R\} + |A^*|(\{U^L\} - \{U^R\})\right] - \sum_S \delta_S \{\overline{G}_V\} \qquad (17)$$

2.2.2 Finite-element structural heat transfer equations

The method of weighted residuals is applied to Eq. (5), over the element domain, Ω, by assuming a linear distribution of the conservation variable U_T, and the flux components E_T and F_T in the form,

$$U_T(x,y,z) = \lfloor N(x,y) \rfloor \{U_T(t)\} \qquad (18a)$$

$$E_T(x,y,z) = \lfloor N(x,y) \rfloor \{E_T(t)\} \qquad (18b)$$

$$F_T(x,y,z) = \lfloor N(x,y) \rfloor \{F_T(t)\} \qquad (18c)$$

where $\lfloor N(x,y) \rfloor$ is the linear interpolation function matrix. The finite element equations can then be derived in the form,

$$[M]\{\Delta U_T\}^{n+1} = \{R_T\}_1^n + \{R_T\}_2^n \qquad (19)$$

where $[M]$ is the mass matrix, $\{\Delta U_T\}^{n+1} = \{U_T\}^{n+1} - \{U_T\}^n$ at time n+1. The $\{R_T\}_1^n$ and $\{R_T\}_2^n$ vectors are associated with the thermal fluxes within element and across element boundary, respectively, and are given by,

$$\{R_T\}_1^n = \int_\Omega \left\{\frac{\partial N}{\partial x}\right\} \lfloor N \rfloor d\Omega \{E_T^n\} + \int_\Omega \left\{\frac{\partial N}{\partial y}\right\} \lfloor N \rfloor d\Omega \{F_T^n\} \qquad (20)$$

$$\{R_T\}_2^n = -\int_{\Gamma_e} \{N\}(E_T^n n_x + F_T^n n_y)\, d\Gamma \qquad (21)$$

2.2.3 Finite-element structural equations

The Galerkin finite element method is applied to Eq. (9) in the same fashion as in the structural heat transfer analysis. The finite element equations can also be derived in the form,

$$[K]\{U_S\} = \{R_S\} + \{R_T\} \qquad (22)$$

where $[K]$ is the stiffness matrix, $\{U_S\}$ is the nodal displacement vector, $\{R_S\}$ is the external load vector and $\{R_T\}$ is the thermal load vector. These matrices are defined by,

$$[K] = \int_\Omega [B]^T [C][B] d\Omega \qquad (23)$$

$$\{R_S\} = \int_{\Gamma_e} [N]^T \{F_S\}\, d\Gamma \qquad (24)$$

$$\{R_T\} = \int_\Omega [B]^T [C] \alpha (T - T_o)\, d\Omega \qquad (25)$$

where $[B]$ is the strain-interpolation matrix, $[C]$ is the elastic modulus matrix, $\{F_S\}$ is the surface traction matrix, α is the thermal expansion coefficient, and T_0 is the reference temperature for zero stress state.

2.3 Solution sequence

The solution sequence developed for fluid-thermal-structural analysis in this paper is based on the fact that the high-speed flow approaches steady-state condition in a much shorter time than that required for the thermal and structural response of structure. Typically, heating rates approach steady state in about a millisecond. At this time, the structural configuration remains undeformed at temperatures only slightly higher than the initial temperature. After a few second, structural temperatures begin to rise appreciably and significant deformation may occur. At this time, thermal and deformation coupling effects alter the flow field. The coupling effects continue to alter the flow and structure behavior until the structure reaches thermal equilibrium.

Based on the above sequence of events, the analysis procedure of high-speed flow-structure interaction consists of the solution sequence as described by Fig. 3. At the initial time, t = 0, the adaptive cell-centered finite element method is first used to predict the high-speed flow behavior as denoted by FA. The flow analysis generates aerothermal loads that include heating rate and pressure along the structural surface. After a short interval of time at $t = t_1$, the predicted aerodynamic heating rate is applied to the structural configuration and structural heat transfer analysis as denoted by TA is used to solve for the structural temperature. Both the structural temperature and the fluid pressure are then used to predict the structural response for deformations and stresses as denoted by SA. The same sequence is repeated to predict the new flow field behavior, the aerothermal loads, the structural temperature, as well as the new structural deformation and stress.

3. Adaptive meshing technique

The idea behind the adaptive meshing technique presented herein is to construct a new mesh based on the solution obtained from the previous mesh. The new mesh will consist small elements in the regions with large change in solution gradients and large elements in the other regions where the change in solution gradients is small. For brevity, description the adaptive meshing technique is omitted herein, but detail can be found in Refs. [4].

4. Application

The capability and efficiency of the method for high-speed flow-structure interaction analysis are evaluated by Mach 10 flow over an inclined plate.

4.1 Mach 10 flow over an inclined plate:

The problem statement of a Mach 10 flow over a 20^O inclined panel is illustrated in Fig. 4(a). The flow enters horizontally through the left boundary of the computational fluid domain and creates an oblique shock wave as highlighted in the figure. The figure illustrates the plate supported by the panel in an initial flat configuration being heated at time t = 0 by high-speed flow. The bottom surface of the panel is assumed perfectly insulated and the top surface is applied by aerodynamic heating rate as illustrated in Fig. 4(b). The panel is constraint on the bottom corners at x = 0.1 and 0.2 m. as shown in Fig. 4(c). For these boundary conditions, the panel deforms into a convex shape after being heated as highlighted in the figure.

The flow-thermal-structural interaction for the inclined plate was analyzed using the solution sequence shown in Fig. 3. At the initial time, t = 0 second, the flow field behavior is predicted by using the cell-centered finite element method. Based on the flow solution obtained from a previous mesh, the adaptive meshing technique as described in the preceding section is then applied to obtain the optimized mesh as shown in Fig. 5 (a). Small elements are automatically generated along the shock line to capture sharp shock resolution and large elements are generated in the other regions where the flow is uniform. The total of 10,611 triangular elements are generated in the inviscid region and 5,050 quadrilateral elements are generated in the boundary layer. Ten graded layers of quadrilateral elements are used in the boundary layer to capture steep temperature gradients for accurate aerodynamic heating rate prediction. Typical flow solution from this adaptive mesh in form of the density contours is presented in Fig. 5 (b) indicating good shock and boundary layer resolution. The structural heat transfer analysis is used to predict the temperature distribution at t = 250 seconds on the panel. At the same time, the quasi-static structural analysis is applied to compute the structural deformation from both the pressure and the thermal load. The panel deforms into the stream, altering the flow significantly by introducing local shocks, expansion regions, and shock boundary-layer interactions. The computational fluid domain is then updated by the deformed structural boundary. The flow field behavior of the new fluid domain is again predicted by using the cell-centered finite element method. The adaptive meshing technique is then applied to generate the optimized mesh as shown in Fig. 6 (a). The adaptive mesh consists of 11,278 triangular elements and 1,910 quadrilateral elements. The shock pattern is altered by convex deformation of constraint panel and small clustered element is automatically generated to capture the

shock line. Ten graded layers of quadrilateral elements are again used in the boundary layer to provide accurate aerodynamic heating rate. The predicted density distribution is obtained as shown in Fig. 6 (b) with curved shock altered by the deformed panel. Figure 7 shows the comparison of the aerodynamic heating rates along the entire plate length at time t = 0 and 250 seconds. Figure 8 shows the predicted pressure distributions along the entire plate length at the same times. These figures show the deformed structure can significantly alter the flow field, and thus the aerodynamic heating rate and pressure load.

5. Concluding Remarks

The adaptive finite element method for flow-structure interaction is presented to analyze the coupled behavior of high-speed compressible flow, structural heat transfer, and structural response. The finite element method based on a cell-centered algorithm is used to predict the high-speed compressible flow behavior. The method is then combined with the adaptive meshing technique to improve the flow accuracy. The technique generates an entirely new mesh based on solution obtained from the previous mesh. The new mesh consists of the clustered elements in the region with large change in the solution gradients to provide the high accuracy and large elements are generated in the other regions to minimize the computational time and computer memory. The Galerkin finite element method is used to predict the structural heat transfer and structural response behaviors. The finite element formulation and computational procedure are presented. Mach 10 flow over an inclined plate was studied to assess the capability and efficiency of the proposed procedure. The application demonstrates that the proposed procedure can provide analysis solution accuracy and computational efficiency for predicting complex flow-thermal-structural behavior of the fluid-structure interaction problems.

6. Acknowledgement

The authors are pleased to acknowledge the Thailand Research Fund (TRF), Bangkok, Thailand, for supporting this research work.

References

[1] Anderson, J. D. Jr., Modern Compressible Flow With Historical Prospective, McGraw-Hill, New York, 1982.

[2] Anderson, J. D. Jr., Fundamentals of Aerodynamics, Second Ed., McGraw-Hill, New York, 1991.

[3] Anderson, J. D. Jr., Computational Fluid Dynamics, McGraw-Hill, New York, 1995.

[4] Limtrakarn, W. and Dechaumphai, P., "Enhanced Compressible Flow Solution by Adaptive Cell-Centered Finite Element Method," Journal of the Chinese Institute of Engineers, 2003, Vol. 26.

[5] Fung, Y. C., Foundations of Solid Mechanics, International Edition, Prentice-Hall, 1965.

[6] Gnoffo, P. A., "Application of Program LAURA to Three-dimensional AOTV Flowfields," AIAA Paper 86-0565, 1986.

[7] Hirsch, C., Numerical Computation of Internal and External Flows, Vol. 1, John Wiley, New York, 1988.

[8] White, F. M., Viscous Fluid Flow, Second Ed., McGraw-Hill, New York, 1991.

[9] Zienkiewicz, O. C. and Taylor, R. L., The Finite Element Method, Fifth Ed., Butterworth-Heinemann, Woburn, MA, 2000.

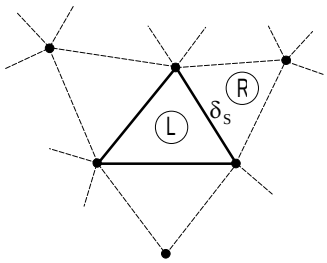

Fig. 1 – The side length, δ_S, between the left element (L) and right element (R).

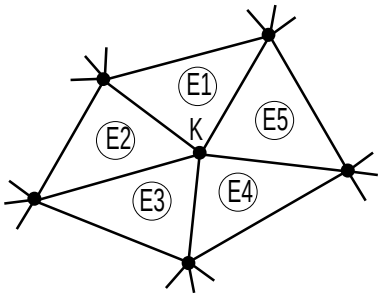

Fig. 2 – Node K is surrounded by a number of elements.

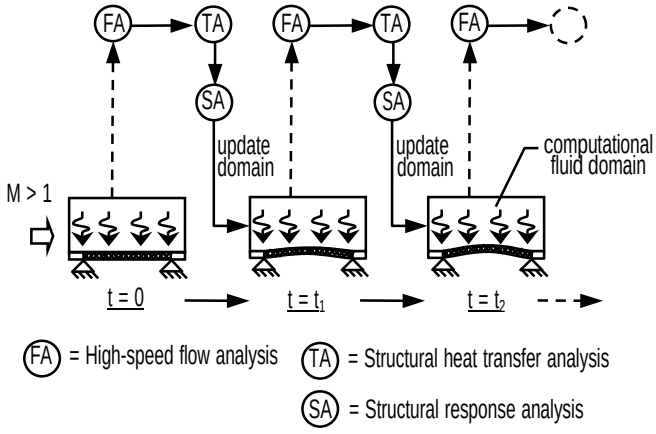

Fig. 3 – Solution sequence of flow-structure interaction for high-speed flow over a flat plate.

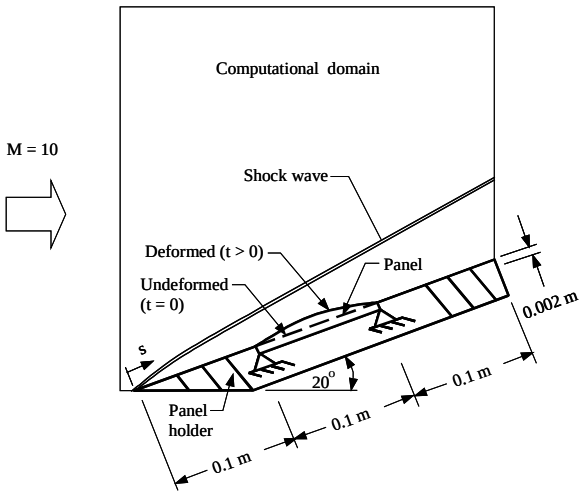

Fig. 4 – Mach 10 flow over an inclined plate.

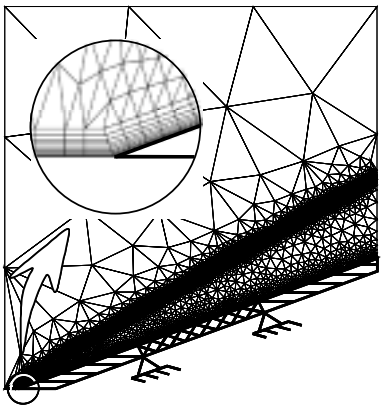

(a) Adaptive mesh

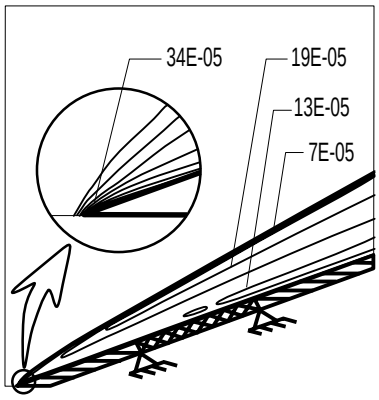

(b) Density distribution

Fig. 5 – Adaptive mesh and corresponding density contours (kg/m^3) for Mach 10 flow over an inclined plate at initial time.

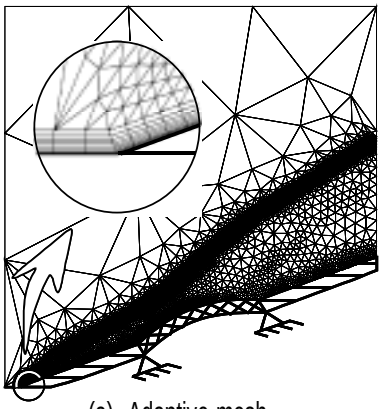

(a) Adaptive mesh

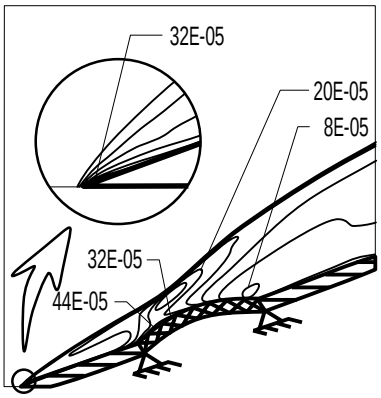

(b) Density distribution

Fig. 6 – Adaptive mesh and corresponding density contours (kg/m^3) for Mach 10 flow over an inclined plate with convex deformation.

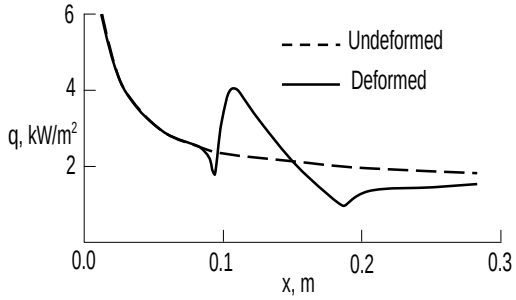

Fig. 7 – Comparative heat flux distributions for Mach 10 flow over the undeformed and deformed panel.

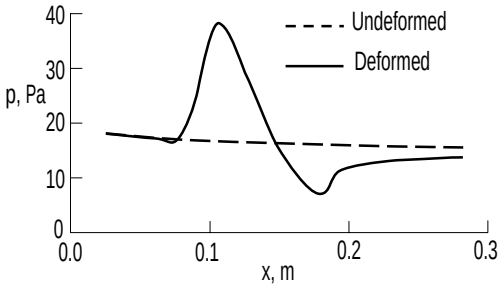

Fig. 8 – Comparative pressure distributions for Mach 10 flow over the undeformed and deformed panel.